Research Article | Vol. 26, No. 19 | 17 Sep 2018 | OPTICS EXPRESS 25003
Optics EXPRESS

Dispersion control for temporal contrast optimization

JERYL TAN,[1,2] NICOLAS FORGET,[3] ANTONIN BOROT,[1,4] DANIEL KAPLAN,[3] PIERRE TOURNOIS,[3,5] ALEXANDER MUSCHET,[1,2] AND LASZLO VEISZ[1,2,*]

[1]*Max-Planck-Institut für Quantenoptik, Hans-Kopfermann Strasse 1, 85748, Garching, Germany*
[2]*Department of Physics, Umeå University, SE-901 87, Umeå, Sweden*
[3]*FASTLITE, 1900 route des Crêtes, 06560 Valbonne, France*
[4]*Service des Photons, Atomes et Molécules, CEA, DSM/IRAMIS, CEN Saclay, 91191, Gif-sur-Yvette, France*
[5]*Deceased 6 March 2017*
**laszlo.veisz@umu.se*

Abstract: We investigate the temporal contrast of the Light Wave Synthesizer 20 (LWS-20): a powerful, few-cycle source based on the optical parametric synthesizer principle. Saturation effects in the RF amplifier driving the acousto-optic programmable dispersive filter (AOPDF) were found to degrade the coherent contrast for non-monotonic group delay corrections. We subsequently present a new dispersion scheme and design a novel transmission grism-based stretcher optimized for LWS-20. The resulting temporal contrast of the amplified, compressed output pulses is improved by 2-4 orders of magnitude compared to the former design.

1. Introduction

Optical Parametric Chirped-Pulse Amplification (OPCPA) and Optical Parametric Synthesizer (OPS) are promising and rapidly developing techniques for the generation of terawatt (TW) level peak power, few-cycle laser pulses for various experiments at the frontiers of nonlinear attosecond science and laser-plasma physics [1–6]. Not surprisingly, dispersion needs to be carefully managed over the entire spectral range in order to compress pulses to the few-cycle regime and below [1,7,8]. While much effort has been devoted to carefully optimizing the proper stretcher and compressor over the past few decades [8–14], there still remains higher-order residual spectral phase terms of various origins that need to be compensated for. Therefore, adaptive-programmable pulse compression remains useful and widespread for few-cycle laser systems, via e.g. liquid-crystal spatial light modulators [15,16] or acousto-optic programmable dispersive filters (AOPDFs) [17,18]. The AOPDF or "Dazzler" (Fastlite) remains advantageous over the former due to its extremely compact setup, intrinsic stability (especially with regard to carrier-envelope phase), wide dynamic range (>45 dB), implementation flexibility (i.e. no need to spatially disperse spectral components beforehand) and continuous spectral phase modulation [17,18].

Nonetheless, the effect of the acousto-optic interaction in an AOPDF on the high-dynamic-range temporal contrast of the (amplified) output laser pulse – i.e. the ratio between the intensity of the pulse-preceding background and the main pulse – has not yet been investigated. Alongside the required extremely high intensities and peak powers, the temporal contrast is a crucial laser parameter that needs to be optimized for various relativistic laser-plasma experiments such as ion acceleration [19,20] and different kinds of surface high-harmonic generation [21–23]. Typical CPA or OPCPA systems have a prepulse-pedestal intensity structure of various origins, e.g. amplified spontaneous emission (ASE) [24], amplified parametric superfluorescence [25], imperfect compression or unwanted pulse replica [26]. These prematurely ionize the target prior to the arrival of the main pulse, forming a rapidly expanding pre-plasma that significantly changes the nature of the interaction between the main pulse and the plasma via a longer-than-optimal plasma scale length [27,28].

#338285 https://doi.org/10.1364/OE.26.025003
Journal © 2018 Received 26 Jul 2018; revised 29 Aug 2018; accepted 30 Aug 2018; published 10 Sep 2018

Optics EXPRESS

In this paper, we demonstrate how to optimize the operating conditions of an AOPDF to preserve the temporal pulse contrast of the Light Wave Synthesizer 20 (LWS-20): a sub-two-cycle, 16 TW peak power OPS system reported by Rivas et al. [1]. First, we show that an AOPDF programmed with a non-monotonic group delay (GD) degrades the temporal contrast of output pulses on a picosecond time scale when its driving RF amplifier is saturated (Section 2). We then present a novel grism stretcher designed to cancel material dispersion in the LWS-20 so that the residual GD is monotonic from 580 to 1020 nm and also compatible with the AOPDF compensation capabilities (Section 3). This new dispersion design both optimizes the diffraction efficiency of the AOPDF and makes it robust against RF saturation effects. Supporting pulse cross-correlation measurements indicate improvement by 2 to 4 orders of magnitude of the output pulse contrast in comparison to that with a non-monotonic residual GD (Section 4).

2. Phase-to-amplitude coupling in saturated RF amplifiers

The pulse-shaping mechanism at work in an AOPDF relies on the collinear acousto-optic interaction between an acoustic wave packet and an optical pulse. When the phase-matching conditions are fulfilled, a fraction of the input optical beam is diffracted. The electric field of the diffracted pulses in the time domain can essentially be described as the convolution of an impulse function with the input field, which is simply a rescaled version of the acoustic strain field [17,18]. The pulse shaping accuracy of an AOPDF is therefore directly linked to that of the RF signal driving the transducer. Clearly, spurious distortions of the driving RF signal can be transferred to the diffracted pulses. In particular, a poor signal-to-noise ratio can result in spurious amplitude and phase contributions in the optical domain - in other words - may degrade the pulse contrast. In practice, the RF signal is generated by an arbitrary waveform generator and then amplified by a broadband AB-class RF amplifier. Like any physical amplifier, the RF amplifier is subject to saturation effects which can be interpreted in the time-domain as distortions of the carrier and of the envelope. These effects can also interpreted in the frequency domain as instantaneous nonlinear effects of various orders such as second or third harmonic generation. However, in contrast to optical nonlinear effects, there is no notion of phase-matching nor of selection by symmetry considerations in electronic RF amplifiers. As a consequence, all possible nonlinear effects occur simultaneously. Of particular interest is phase-to-amplitude coupling, which distorts the RF spectral amplitude whenever the second-order derivative of the RF spectral phase vanishes.

To illustrate this behavior, we sample the RF waveform at the output of a 50-W RF amplifier with a 500-MHz oscilloscope (Waverunner, LeCroy) and compare the waveform as a function of the RF gain. Rather than showing the time-dependent voltage, which is barely readable, we display the RF spectral amplitude as a function of gain (Fig. 1). In this case, the input RF spectrum spans from ~65 to ~130 MHz with a rectangular shape, and the spectral phase is a single-cycle cosine. As the RF amplifier gain is increased, the spectral intensity gets heavily modulated and new frequency components appear around 50 MHz and 150 MHz. These new frequencies are not phase-matched to any of the input optical wavelengths (0.5-1.0 µm) and do not contribute to the acousto-optic diffraction. However, the fast RF amplitude modulations within the 65-130 MHz bandwidth are transferred to the output diffracted beam through acousto-optic diffraction. To understand this behavior, we compute the spectrograms (windowed Fast Fourier transform) of the RF waves as a function of gain. Since the duration of the RF wave (~25 µs) is several orders of magnitude longer than the electrical carrier (>7 ns), the frequency-content of a “slice” at a given delay is very well defined. Thus, one can use the vocabulary developed for wave packets satisfying the slowly-varying envelope approximation, in particular the notions of instantaneous frequency and group delay.

Optics EXPRESS

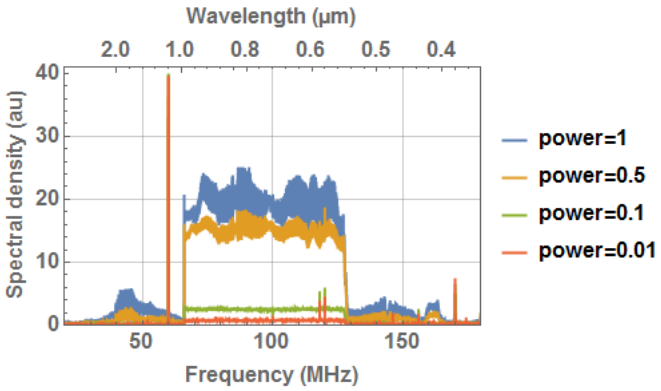

Fig. 1. Spectral density of the amplified RF waves as a function of gain. P = 0 corresponds to no amplification, while P = 1 corresponds to the maximum gain (i.e. the maximum output RF peak power of 50 W). Spikes at ~60 MHz and harmonics (~120 MHz and ~180 MHz) are weak continuous leakages from the generation card. Saturation effects appear at P>0.1 as high-frequency spectral modulations and nonlinear mixing processes generate new frequencies.

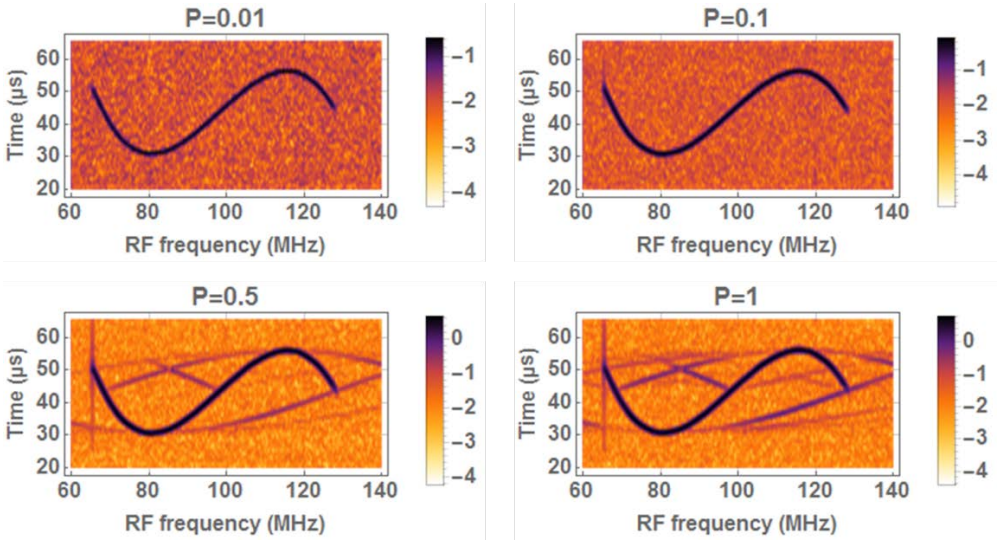

Fig. 2. RF spectrograms (log scale) of the amplified RF waves as a function of RF gain (P). P = 0 corresponds to no gain, while P = 1 corresponds to maximum gain. Additional parasitic frequencies appear at high gain as a result of four-wave and higher-order wave mixing in the RF amplifier.

At low RF power levels, the RF group delay (RF-GD) is well defined in the sense that a group delay can be attributed unambiguously to each RF frequency. As expected, the RF-GD is a single-cycle sine wave with a frequency range of ~65 MHz to ~130 MHz and a total delay of ~25 μs (Fig. 2). As the RF power is increased, the diffraction efficiency also increases linearly but new frequencies are generated – particularly in the temporal vicinity of the RF-GD extrema – and form parasitic RF-GD curves. This phenomenon can be understood from four-wave mixing processes such as $\omega_1 + \omega_2 - \omega_3 \rightarrow \omega_4$. For example, the frequencies at ~75 MHz and ~85 MHz, which are simultaneously present at 33-34 μs, beat and generate 2*75-85 = 65 MHz and 2*85-75 = 95 MHz. More generally, in the vicinity of a RF-GD extremum, four-wave mixing generates new frequencies along a parabola tangent to the extremum with a curvature three times smaller. At even higher RF powers, one can notice the onset of effects of even higher-order wave mixing (e.g. a second 6th-order tangent parabola).

Optics EXPRESS

As a result, some frequencies appear at multiple delays (e.g. 110 MHz appears at both ~35 µs and ~55 µs) which give rise to complex pre-/post-pulses in the time-domain. To assess the contrast degradation over the full spectral range, we compute the optical impulse function of the AOPDF as a function of RF power (Fig. 3). In the worst case (i.e. at 100% RF power), a large prepulse-pedestal peaks at ~4.3 ps with an intensity of ~4 orders of magnitude below the main pulse.

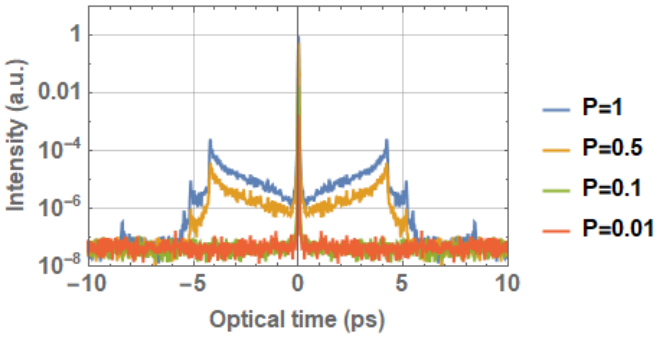

Fig. 3. Temporal structure of the diffracted electric field (D_z) assuming a perfect compression. The contrast degrades to 10^{-3}-10^{-4} as the RF power is increased from 0 to 1.

To conclude this section, using saturated RF amplifiers to drive AOPDFs can significantly degrade the pulse contrast of the shaped output optical pulses. Apart from staying within the linear RF amplification range, which would imply oversized amplifiers and/or be limited by the current commercial technology or total cost, phase-to-amplitude effects can be avoided or strongly mitigated by programming strictly monotonic RF-GDs. This criterion is also optimal with regard to the diffraction efficiency of the AOPDF [29]. A practical consequence is that the applied pulse shaping function should also be a monotonic optical group delay.

3. Design and characterization of a transmission grism stretcher

As detailed by Dou *et al* [8], the LWS-20 is based on a down-chirped amplification scheme involving a grism pair as a stretcher and glass blocks as a compressor. The grism pair was designed to match the dispersion of the compressor up to the third order. The residual spectral phase was then pre-compensated by an AOPDF. However, it was not possible to have a monotonic residual group delay falling within the compensation range of the AOPDF with this stretcher. This motivated the design of a novel, transmission-grating-based grism stretcher, which is described and characterized in the following section. The stretcher (Fig. 4) consists of two parallel transmission gratings of groove density σ at a distance D apart as well as an anti-symmetrically positioned pair of isosceles prisms of refractive index $n_P(\lambda)$ and apex angle θ_A – inserted at a tilt angle θ_T between the gratings. d_i and d_o are the separations between the inner and outer prism faces respectively. Thus, the stretcher is almost similar to that reported by [12], with the addition of θ_T to expand the solution space during numerical optimization.

Propagating from left to right, the beam incident upon the first grating at angle θ_0 is diffracted at an angle θ_1 according to the grating equation:

$$\sin\theta_1(\lambda) = \sin\theta_0 + \sigma\lambda \tag{1}$$

where only the most intense order of diffraction (m = −1) is used in this design. The remaining propagation angles θ_2 to θ_5 are linked by Snell's law and simple geometric considerations:

Optics EXPRESS

$$\theta_2(\lambda) = \theta_1(\lambda) - \theta_T \tag{2}$$

$$n_P(\lambda)\sin\theta_3(\lambda) = \sin\theta_2(\lambda) \tag{3}$$

$$\theta_4(\lambda) = \theta_3(\lambda) - \theta_A \tag{4}$$

$$n_P(\lambda)\sin\theta_4(\lambda) = \sin\theta_5(\lambda) \tag{5}$$

Note the use of the signed-angle convention: θ is positive if measured counter-clockwise from the respective surface (i.e. θ_A, θ_1, θ_2, and θ_3) and negative if clockwise (i.e. θ_T, θ_0, θ_4 and θ_5). The rooftop mirror after the second grating reflects the beam perpendicularly through the stretcher at a different height, thereby double-passing the grism pair.

The optical group delay introduced by a double-pass through the stretcher, GD_{str}, is derived using similar analytical ray-tracing calculation methods by [12,30]:

$$\begin{aligned}\frac{c\,GD(\lambda)}{2} = {} & \frac{d_i}{\cos\theta_5(\lambda)} + [D - d_x]\left[\frac{1-\cos[\theta_1(\lambda)-\theta_0]}{\cos\theta_1(\lambda)}\right] \\ & + \frac{1}{\cos\theta_3(\lambda)}\left[d_o - d_i\frac{\cos[\theta_5(\lambda)+\theta_A]}{\cos\theta_5(\lambda)}\right] \\ & \times\left[n_g(\lambda) - \frac{\cos\theta_4(\lambda)}{\sin\theta_A\cos\theta_1(\lambda)}[\sin\theta_0\cos\theta_2(\lambda) - \sin\theta_T]\right]\end{aligned} \tag{6}$$

where $n_g(\lambda)$ is the group index of the prisms and d_x is the horizontal separation between the prism apices:

$$d_x = [d_o\sin(\theta_A + \theta_T) - d_i\sin(\theta_T)]/\sin(\theta_A) \tag{7}$$

Equation (6) can be understood as follows: the first term is the GD acquired from propagation through the air gap between the prisms; the second term is the GD for a transmission grating pair [30] separated by a distance $D - d_x$; and the third term is a correction term that accounts for the beam propagation through the prisms as well as the vertical beam shift between the prism apices.

Hence the stretcher is fully parameterized from a design standpoint after defining the groove density and incidence angle of the grating, the refractive index of the glass prism, and optimizing the 5 independent geometric parameters D, d_i, d_o, θ_A & θ_T. In our design, the numerical optimization for a monotonic residual GD is carried out via the gradient descent algorithm for the same material parameters as in the LWS-20, which comprises mostly of the glass compressor (160 mm of SF57 and 100 mm of Quartz) and the Dazzler crystal (45 mm of TeO_2) [1]. The final values of the five geometric parameters are D = 69.5 mm, d_i = 22.9 mm, d_o = 59.6 mm, θ_A = 54.52°, and θ_T = –39.23°. The custom-made, surface-relief etched fused silica transmission gratings (30 x 15 mm^2, Ibsen Photonics) have a groove density σ = 966.2 grooves/mm, design incidence angle θ_0 = –20° and are optimized for the m = –1 diffraction order. The prisms are also custom-made from N-SF57 glass (Eksma Optics) and are antireflection-coated on both isosceles faces, so that the average reflection for p-polarized light is <2% per face over the target spectral range (580 – 1020 nm) for the incidence and refraction angles in our design.

Optics EXPRESS

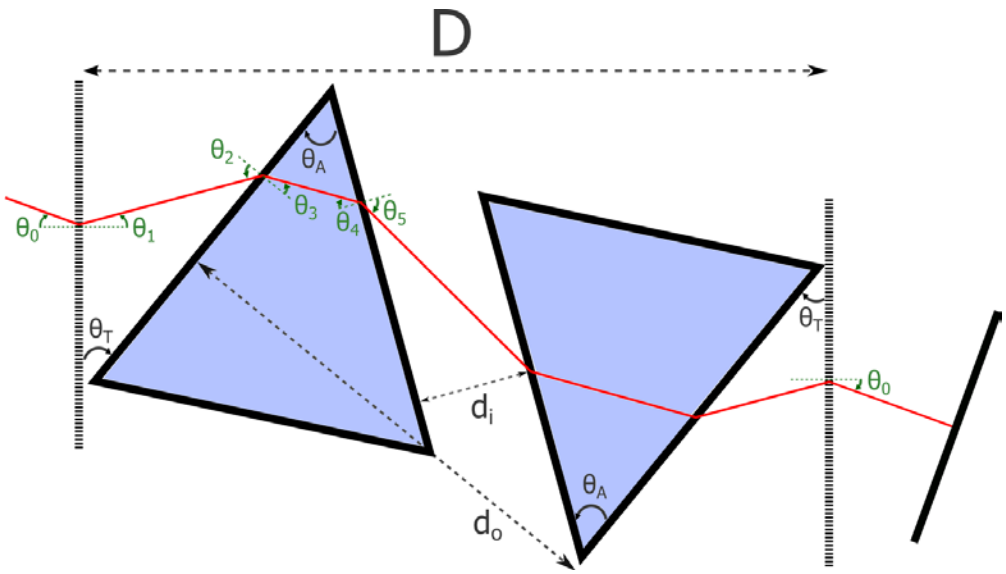

Fig. 4. Optical path of an arbitrary frequency component within the stretcher. Propagation angles (green) are numbered sequentially from left to right: $\theta_{0,1,2,3,4,5}$ from the incidence angle of the first grating up until the air gap between the prisms, then $\theta_{5,4,3,2,1,0}$ from the air gap until the output of the second grating. The rooftop mirror after the second grating enables a double-pass configuration.

The input spectrum into and the output spectrum from the stretcher as depicted in Fig. 5(a) was measured by a spectrometer. To determine the absolute spectral transmission efficiency, the relative spectral transmission – i.e. the output divided by the input spectrum – is rescaled so that the integral over the design spectral range matches the total measured throughput of 19%. The reduced transmission at the edges of the spectral range is primarily attributed to the diffraction efficiency of the transmission grating and to the AR-coatings on the prisms.

A simulation of the resulting residual GD is plotted in Fig. 5(b) together with the stretcher GD and the total material GD in the LWS-20 for reference. It can be seen that the total residual GD in the design spectral range falls within the Dazzler compensation range (≈17 ps) and is monotonic everywhere. This is made possible by the extra degree of freedom θ_T compared to the previous designs [8, 12] as well as the increased Dazzler compensation range.

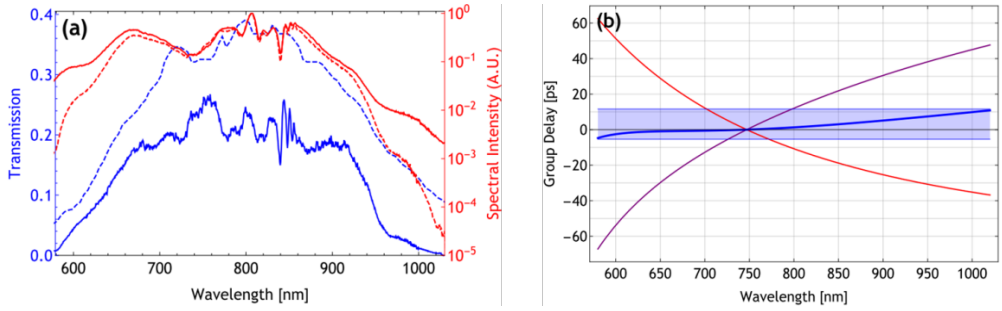

Fig. 5. (a) Measured absolute spectral transmission (solid blue) of the stretcher over the design spectral range of 580 – 1020 nm, plotted together with the normalized input spectra (solid red), output spectra (dashed red) and grating-only transmission for p-polarization after 4 passes (dashed blue). (b) Simulated GD vs wavelength curves. The residual GD (blue) – i.e. the sum of the total material GD in LWS-20 (red) plus the stretcher GD (purple) – is strictly monotonic and falls within the Dazzler compensation range of ≈17 ps (light blue rectangle).

Optics EXPRESS

4. Further experimental results

To measure the residual GD, the amplified pulses in the LWS-20 are adaptively compressed with the aid of a chirp-scan trace [31], which iteratively programs the Dazzler GD until the residual GD is fully compensated. Pulse compression to the sub-5-fs regime is additionally confirmed by the single-shot frequency-resolved optical gating (FROG) and single-shot second-harmonic autocorrelation (SHAC) techniques [1]. The measured residual GDs with the new stretcher are plotted in Fig. 6(a) together with that of the Dou stretcher for reference.

In addition, the temporal intensity structure of the compressed pulses is characterized using a home-made third-harmonic cross-correlation setup with a dynamic range of up to 9-10 orders of magnitude [32]. It can be seen that the monotonicity of the residual GD curve has a strong effect on the temporal contrast. The simulated temporal contrast degradation (Fig. 3) from the non-monotonic residual GD of the Dou stretcher (red curve, Fig. 6(a)) closely matches the measured contrast (red curve, Fig. 6(b)): there is a prepulse-pedestal peak around t ~4 ps approximately 3 – 4 orders of magnitude smaller than the main pulse. To further investigate this effect, the inter-prism distances in the new stretcher are systematically manipulated so that the residual GD is extremely flat between the two GD extrema (green curve, Fig. 6(a)). The resulting contrast ratio of 10^{-2} – 10^{-3} at t ~1 ps is even worse (green curve, Fig. 6(b)) than in the Dou stretcher. This is due to the stronger beating of many RF frequencies in the Dazzler system that cause stronger spectral amplitude modulations in the RF wave, and hence also in the diffracted optical pulse. Using the new stretcher at the design parameters provided in Section 3, the residual GD is strictly monotonic (black curve, Fig. 6(a)) and the corresponding contrast (black curve, Fig. 6(b)), which is improved by 2 – 4 orders of magnitude below 5 ps, is the best-case scenario.

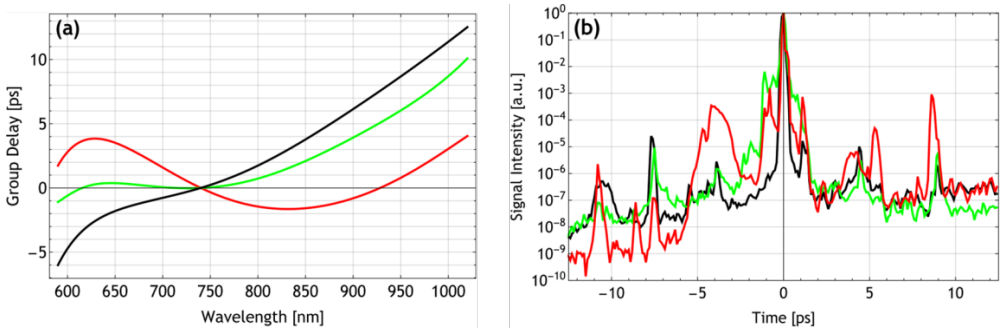

Fig. 6. (a) The residual GD curves for the old stretcher (red), new stretcher at a closer, sub-optimal inter-prism separation (green), and the new stretcher at the optimized inter-prism separation (black). (b) Temporal intensity structure of the compressed output pulse measured by third-order cross-correlation [32]. Note the color correspondence to the residual GD curves in (a). The best contrast results from a monotonic residual GD (black curve).

Further insight can be gained by analyzing the RF waves for the design residual GD of the new stretcher, as previously conducted in Section 2 for the Dou stretcher. Since the curve is monotonic, the acoustic spectrograms indicate that high-order wave mixing is significantly reduced (Fig. 7). The two vertical lines around 118 MHz and 120 MHz at P_{RF} = 0.01 are leaks from the RF generation board, but are not amplified at higher powers. At P_{RF} = 0.5 and P_{RF} = 1, the sharp horizontal and vertical lines at the beginning and end of the wave, which originate from the rectangular RF spectrum, couple with the programmed RF-GD and form a faint, second GD curve around 100 MHz (Fig. 7, P_{RF} = 1). Nonetheless, the intensities of this parasitic curve and of the horizontal and vertical lines are too low to have a measureable effect on the contrast.

Optics EXPRESS

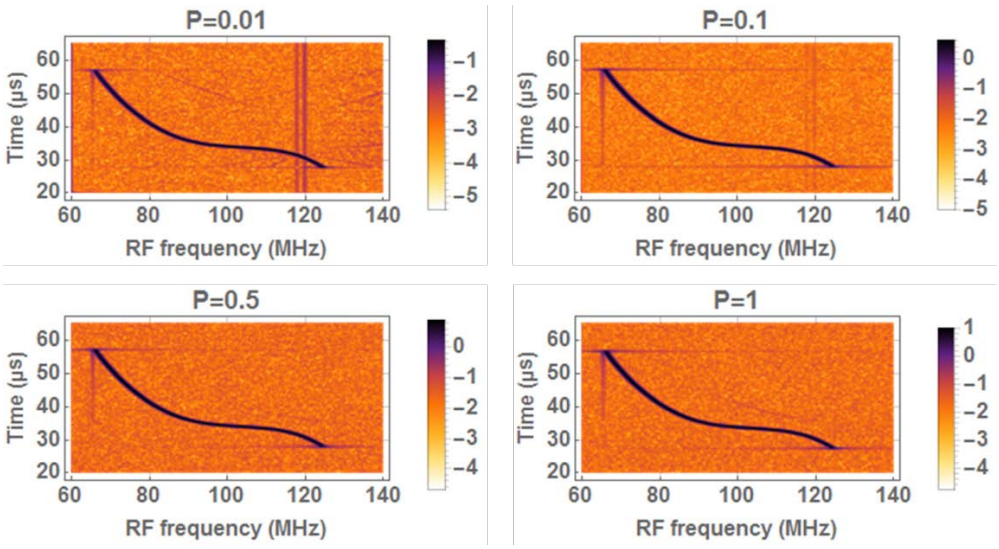

Fig. 7. Acoustic spectrograms (log scale) of the programmed optimal monotonic Dazzler GD for various RF powers. The spectrograms are much cleaner than in the case of the non-monotonic residual GD (Fig. 3). Lines along the frequency and time axes are respectively induced by the spectral shape (rectangular spectrum with sharp edge transitions) and the processing filter (windowed Fourier transform).

5. Conclusion

In conclusion, we have shown that non-monotonic RF waveforms are strongly distorted in saturated RF amplifiers. When such waveforms drive an AOPDF, the temporal contrast of the shaped pulses can be significantly degraded. As a consequence, working within the linear operation range of the AOPDF RF-amplifier is recommended. It is nevertheless possible to operate an AOPDF with a saturated RF amplifier, provided that the programmed group delay is monotonic. In light of this constraint, we designed, optimized and characterized a new transmission grism-based stretcher that – in combination with the dispersion of the other elements of the OPS – achieves a monotonic residual group delay over the target spectral range of the AOPDF. With this new stretcher, the contrast ratio of the output pulse is improved by 2 to 4 orders of magnitude compared to the previous stretcher. This emphasizes the need for proper residual dispersion management in high-power laser systems pushing the frontier of relativistic attosecond science.

Funding

DFG-Project Transregio TR18; Euratom Research and Training Program 2014-2018 (633053); EUROfusion Consortium; The Munich Centre for Advanced Photonics (MAP); Swedish Research Council (2016-05409).

Acknowledgments

We thank the support of Ferenc Krausz.

Disclosures

The authors declare that there are no conflicts of interest related to this article.

References

1. D. E. Rivas, A. Borot, D. E. Cardenas, G. Marcus, X. Gu, D. Herrmann, J. Xu, J. Tan, D. Kormin, G. Ma, W. Dallari, G. D. Tsakiris, I. B. Földes, S.-W. Chou, M. Weidman, B. Bergues, T. Wittmann, H. Schröder, P.

Optics EXPRESS

Tzallas, D. Charalambidis, O. Razskazovskaya, V. Pervak, F. Krausz, and L. Veisz, "Next generation driver for attosecond and laser-plasma physics," Sci. Rep. **7**(1), 5224 (2017).
2. G. Ma, W. Dallari, A. Borot, F. Krausz, W. Yu, G. D. Tsakiris, and L. Veisz, "Intense isolated attosecond pulse generation from relativistic laser plasmas using few-cycle laser pulses," Phys. Plasmas **22**(3), 033105 (2015).
3. S. Kühn, M. Dumergue, S. Kahaly, S. Mondal, M. Füle, T. Csizmadia, B. Farkas, B. Major, Z. Várallyay, E. Cormier, M. Kalashnikov, F. Calegari, M. Devetta, F. Frassetto, E. Månsson, L. Poletto, S. Stagira, C. Vozzi, M. Nisoli, P. Rudawski, S. Maclot, F. Campi, H. Wikmark, C. L. Arnold, C. M. Heyl, P. Johnsson, A. L'Huillier, R. Lopez-Martens, S. Haessler, M. Bocoum, F. Boehle, A. Vernier, G. Iaquaniello, E. Skantzakis, N. Papadakis, C. Kalpouzos, P. Tzallas, F. Lépine, D. Charalambidis, K. Varjú, K. Osvay, and G. Sansone, "The ELI-ALPS facility: the next generation of attosecond sources," J. Phys. At. Mol. Opt. Phys. **50**(13), 132002 (2017).
4. E. J. Takahashi, P. Lan, O. D. Mücke, Y. Nabekawa, and K. Midorikawa, "Infrared two-color multicycle laser field synthesis for generating an intense attosecond pulse," Phys. Rev. Lett. **104**(23), 233901 (2010).
5. Y. Nabekawa, Y. Furukawa, T. Okino, A. Amani Eilanlou, E. J. Takahashi, K. Yamanouchi, and K. Midorikawa, "Sub-10-fs control of dissociation pathways in the hydrogen molecular ion with a few-pulse attosecond pulse train," Nat. Commun. **7**, 12835 (2016).
6. S. Huang, G. Cirmi, J. Moses, K. Hong, S. Bhardwaj, J. R. Birge, L. Chen, E. Li, B. J. Eggleton, G. Cerullo, and F. X. Kärtner, "High-energy pulse synthesis with sub-cycle waveform control for strong-field physics," Nat. Photonics **5**(8), 475–479 (2011).
7. S. Chia, G. Cirmi, S. Fang, G. M. Rossi, O. D. Mücke, and F. X. Kärtner, "Two-octave-spanning dispersion-controlled precision optics for sub-optical-cycle waveform synthesizers," Optica **1**(5), 315–322 (2014).
8. T. H. Dou, R. Tautz, X. Gu, G. Marcus, T. Feurer, F. Krausz, and L. Veisz, "Dispersion control with reflection grisms of an ultra-broadband spectrum approaching a full octave," Opt. Express **18**(26), 27900–27909 (2010).
9. D. Strickland and G. Mourou, "Compression of amplified chirped optical pulses," Opt. Commun. **56**(3), 219–221 (1985).
10. F. Tavella, Y. Nomura, L. Veisz, V. Pervak, A. Marcinkevičius, and F. Krausz, "Dispersion management for a sub-10-fs, 10 TW optical parametric chirped-pulse amplifier," Opt. Lett. **32**(15), 2227–2229 (2007).
11. J. Zheng and H. Zacharias, "Design considerations for a compact grism stretcher for non-collinear optical parametric chirped-pulse amplification," Appl. Phys. B **96**(2–3), 445–452 (2009).
12. N. Forget, V. Crozatier, and P. Tournois, "Transmission Bragg-grating grisms for pulse compression," Appl. Phys. B **109**(1), 121–125 (2012).
13. S. Grabielle, N. Forget, and P. Tournois, "Tilted transmission grisms for pulse compression with dispersion control up to the fourth order," in *CLEO: Science and Innovations*, Optical Society of America (2014), paper SW1E.6.
14. A. Jullien, A. Ricci, F. Böhle, J. P. Rousseau, S. Grabielle, N. Forget, H. Jacqmin, B. Mercier, and R. Lopez-Martens, "Carrier-envelope-phase stable, high-contrast, double chirped-pulse-amplification laser system," Opt. Lett. **39**(13), 3774–3777 (2014).
15. T. Feurer, J. C. Vaughan, R. M. Koehl, and K. A. Nelson, "Multidimensional control of femtosecond pulses by use of a programmable liquid-crystal matrix," Opt. Lett. **27**(8), 652–654 (2002).
16. S. Witte, R. T. Zinkstok, A. L. Wolf, W. Hogervorst, W. Ubachs, and K. S. E. Eikema, "A source of 2 terawatt, 2.7 cycle laser pulses based on noncollinear optical parametric chirped pulse amplification," Opt. Express **14**(18), 8168–8177 (2006).
17. P. Tournois, "Acousto-optic programmable dispersive filter for adaptive compensation of group delay time dispersion in laser systems," Opt. Commun. **140**(4–6), 245–249 (1997).
18. F. Verluise, V. Laude, Z. Cheng, C. Spielmann, and P. Tournois, "Amplitude and phase control of ultrashort pulses by use of an acousto-optic programmable dispersive filter: pulse compression and shaping," Opt. Lett. **25**(8), 575–577 (2000).
19. B. M. Hegelich, B. J. Albright, J. Cobble, K. Flippo, S. Letzring, M. Paffett, H. Ruhl, J. Schreiber, R. K. Schulze, and J. C. Fernández, "Laser acceleration of quasi-monoenergetic MeV ion beams," Nature **439**(7075), 441–444 (2006).
20. R. A. Loch, T. Ceccotti, F. Quéré, H. George, G. Bonnaud, F. Réau, P. D'Oliveira, M. J. H. Luttikhof, F. Bijkerk, K.-J. Boller, G. Blaclard, and P. Combis, "Ion acceleration in the transparent regime and the critical influence of the plasma density scale length," Phys. Plasmas **23**(9), 093117 (2016).
21. P. Monot, G. Doumy, S. Dobosz, M. Perdrix, P. D'Oliveira, F. Quéré, F. Réau, P. Martin, P. Audebert, J. C. Gauthier, and J. P. Geindre, "High-order harmonic generation by nonlinear reflection of an intense high-contrast laser pulse on a plasma," Opt. Lett. **29**(8), 893–895 (2004).
22. C. Thaury, F. Quéré, J.-P. Geindre, A. Levy, T. Ceccotti, P. Monot, M. Bougeard, F. Réau, P. D'Oliveira, P. Audebert, R. Marjoribanks, and P. H. Martin, "Plasma mirrors for ultrahigh-intensity optics," Nat. Phys. **3**(6), 424–429 (2007).
23. D. An der Brügge and A. Pukhov, "Enhanced relativistic harmonics by electron nanobunching," Phys. Plasmas **17**(3), 033110 (2010).
24. D. Herrmann, L. Veisz, R. Tautz, F. Tavella, K. Schmid, V. Pervak, and F. Krausz, "Generation of sub-three-cycle, 16 TW light pulses by using noncollinear optical parametric chirped-pulse amplification," Opt. Lett. **34**(16), 2459–2461 (2009).
25. S. Witte and K. S. E. Eikema, "Ultrafast optical parametric chirped-pulse amplification," IEEE J. Sel. Top. Quantum Electron. **18**(1), 296–307 (2012).

Optics EXPRESS

26. N. V. Didenko, A. V. Konyashchenko, A. P. Lutsenko, and S. Y. Tenyakov, "Contrast degradation in a chirped-pulse amplifier due to generation of prepulses by postpulses," Opt. Express **16**(5), 3178–3190 (2008).
27. S. Kahaly, S. Monchocé, H. Vincenti, T. Dzelzainis, B. Dromey, M. Zepf, P. Martin, and F. Quéré, "Direct observation of density-gradient effects in harmonic generation from plasma mirrors," Phys. Rev. Lett. **110**(17), 175001 (2013).
28. F. Dollar, P. Cummings, V. Chvykov, L. Willingale, M. Vargas, V. Yanovsky, C. Zulick, A. Maksimchuk, A. G. R. Thomas, and K. Krushelnick, "Scaling high-order harmonic generation from laser-solid interactions to ultrahigh intensity," Phys. Rev. Lett. **110**(17), 175002 (2013).
29. N. T. Form, R. Burbidge, J. Ramon, and B. J. Whitaker, "Parameterization of an acousto-optic programmable dispersive filter for closed-loop learning experiments," J. Mod. Opt. **55**(1), 197–209 (2008).
30. P. Tournois, "New diffraction grating pair with very linear dispersion for laser pulse compression," Electron. Lett. **29**(16), 1414–1415 (1993).
31. V. Loriot, G. Gitzinger, and N. Forget, "Self-referenced characterization of femtosecond laser pulses by chirp scan," Opt. Express **21**(21), 24879–24893 (2013).
32. F. Tavella, K. Schmid, N. Ishii, A. Marcinkevičius, L. Veisz, and F. Krausz, "High-dynamic range pulse-contrast measurements of a broadband optical parametric chirped-pulse amplifier," Appl. Phys. B **81**(6), 753–756 (2005).